True-amplitude Common-offset, Common-azimuth $v(z)$ Migration

YU ZHANG *, SAM GRAY †, AND JERRY YOUNG ‡

Abstract. We investigate the amplitude behavior of common-offset phase-shift migration in two and three dimensions. By transforming phase-shift migration into an equivalent Kirchhoff migration, we find the deviation of the phase-shift migration operator from "true-amplitude." We also investigate the amplitude error introduced by anti-aliasing, for both phase-shift and Kirchhoff migration. Even for fairly routine acquisition characteristics, this amplitude error can dominate the error due to the lack of true-amplitude migration weights, making the analysis of migrated amplitudes problematic, especially for shallow reflection events.

1. Introduction. Reliable migrated amplitudes depend on acquisition geometry, complexity of geologic structure, and choice of migration algorithm. Towed-streamer marine acquisition typically involves a narrow range of azimuth angles, and lends itself well to processing of common-offset, common-azimuth data volumes. When geologic structure is simple, with relatively little variation of lateral velocity, using a migration algorithm that is correct for $v(z)$ often provides reasonable amplitudes for post-migration amplitude-vs.-offset (AVO) analysis. This is true for a gently varying background medium, possibly even when the structures being imaged have significant dip. Presently, several algorithms are in use for $v(z)$, common-offset, common-azimuth migration, with Kirchhoff migration weights providing known "true" amplitudes. Schleicher et al. (1993) and Bleistein et al. (2000) have provided general true-amplitude weights for Kirchhoff migration. Winbow and Schneider (1999) specialized these weights for $v(z)$ and shown their importance in realistic settings. Zhang et al. (2000) modified the $v(z)$ weights, greatly simplifying them in the interest of speeding up their calculation and use in a production Kirchhoff migration program.

Before these true-amplitude weights and their approximations appeared, Dubrulle (1983) presented a common-offset phase-shift migration method with no discussion of amplitudes. Ekren and Ursin (1999) attached amplitudes to this method, and used it to provide migrated input to AVO analysis in two dimensions. Dubrulle's method extends readily to three dimensions, and we discuss the amplitude behavior of both the two-dimensional (2-D) and three-dimensional (3-D) versions of this method. In particular, by performing a stationary-phase analysis of Dubrulle's method in two and three dimensions, we show that the weights implied in this method, modified by a geometrical spreading correction, are equivalent to "true" Kirchhoff migration weights for all dips at zero offset and for a flat reflector at all offsets. We also show that for constant velocity and nonzero offset case, the amplitude error caused by Dubrulle's phase-shift migration is small, within 6.1%. Etgen (1998) provided the modifications needed to include true amplitudes in Dubrulle's 3-D method, with the resulting migration method having the speed of phase-shift migration and the true-amplitude behavior of Kirchhoff migration.

An additional, often neglected, factor affecting migrated amplitudes is anti-aliasing (Gray, 1992; Lumley et al., 1994). Anti-aliasing reduces the frequency content of an input trace as it swings out to steeper angles under the action of migration. As frequencies are successively removed from the trace, the trace suffers amplitude loss as well, with different offsets losing amplitude at different rates at a given dip angle. We show that, if the input data have frequency content above the aliasing frequency, migration anti-aliasing can distort migrated amplitudes. In this case, the amplitude distortion due to anti-aliasing (whether implicitly applied as part of the phase-shift migration algorithm, or "manually" applied as part of a Kirchhoff migration program) can dominate the amplitude distortion due to the lack of true-amplitude weighting in the migration.

*VeritasDGC Inc., 10300 Town Park, Houston, TX 77072 (yu_zhang@veritasdgc.com).

†Veritas DGC Inc., 2200, 715 5th Avenue, Calgary, AB, Canada T2P 5A2 (sam_gray@veritasdgc.com).

‡ VeritasDGC Inc., 10300 Town Park, Houston, TX 77072 (jerry_young@veritasdgc.com).

2. Dubrulle's common-offset migration. In this section we introduce Dubrulle's (1983) 2-D common-offset phase-shift migration, and then we generalize it to 3-D.

For 2-D common-offset phase-shift migration, the input data $U(x_m, z=0; t)$ depends on time t, midpoint x_m and half offset h; the migrated image $R(x,z) = U(x,z;t=0)$ corresponds to a diffractor at (x,z). Dubrulle's phase-shift migration is based on the following geometrical interpretation (Ekren and Ursin, 1999). Starting from a space-time diffractor response in a $v(z)$-layered medium, the response is accumulated into the migration image by summing data along the line tangent to the response at the sample location (x,t) (Figure 1).

Defining the 2-D Fourier transform pair

$$\hat{F}(k_x;\omega) = \iint F(x;t) e^{-ixk_x} e^{-it\omega} dx dt, \qquad \text{forward}$$

and

$$F(x;t) = \frac{1}{(2\pi)^2} \iint \hat{F}(k_x;\omega) e^{ixk_x} e^{it\omega} dk_x d\omega, \qquad \text{inverse}$$

we can formulate Dubrulle's phase-shift migration method as

$$U(x,z;t) = \frac{1}{(2\pi)^2} \iint \hat{U}(k_x, z=0;\omega) e^{ik_x x} e^{i\omega(t+t_0)} dk_x d\omega. \tag{2.1}$$

In this equation,

$$t_0 = \tau(x, x_m; z) - p_x(x_m - x),$$

$\tau(x, x_m; z)$ is the travel time from the source $(x_m - h, 0)$ to the diffractor (x,z) and back to the receiver $(x_m + h, 0)$, and

$$p_x = \frac{d\tau}{dx_m}$$

is the slope of the tangent of traveltime at x_m. The slope p_x corresponds to a plane-wave $e^{i(k_x x_m + \omega t)}$ by the relationship

$$p_x = -\frac{k_x}{\omega}.$$

In following derivation and analysis, we use $\tilde{U}(x,z;\omega)$ to distinguish single Fourier transform in time

$$\tilde{U}(x,z;\omega) = \int U(x,z;t) e^{-it\omega} dt.$$

Dubrulle's method can be generalized easily to migrate 3-D common-offset, common-azimuth data $U(x_m, y_m, z=0; t)$ by the following generalization of (2.1):

$$U(x,y,z;t) = \frac{1}{(2\pi)^3} \iiint \hat{U}(k_x, k_y, z=0;\omega) e^{i(k_x x + k_y y)} e^{i\omega(t+t_0)} dk_x dk_y d\omega, \tag{2.2}$$

where

$$t_0 = \tau(x, y, x_m, y_m; z) - p_x(x_m - x) - p_y(y_m - y),$$

and

$$p_x = \frac{\partial \tau}{\partial x_m} = -\frac{k_x}{\omega} \quad \text{and} \quad p_y = \frac{\partial \tau}{\partial y_m} = -\frac{k_y}{\omega}.$$

To simplify our discussion below, we will assume that in 3-D, the shot-receiver pairs are parallel to the direction of y (or y_m), i.e. they are assigned the coordinates $(x_m - h, y_m)$ and $(x_m + h, y_m)$, respectively.

3. Amplitude performance of zero-offset phase-shift migration. When the offset is zero, Dubrulle's formula reduces to Gazdag's (1978) phase-shift migration. So we begin with Gazdag's migration, and discuss its amplitude performance in the constant velocity case:

$$\hat{U}(k_x, z; \omega) = \hat{U}(k_x, z = 0; \omega) e^{i \frac{2\omega z}{v} \sqrt{1 - \frac{k_x^2 v^2}{4\omega^2}}}. \tag{3.1}$$

This simple case sheds light on the basic ideas of this paper.

Inverse Fourier transforming (3.1) into space and time, we obtain

$$U(x, z; t) = \frac{1}{\pi} \frac{\partial}{\partial z} \left(U(x, z = 0; t) * \frac{H(\tau + t)}{\sqrt{\tau^2 - t^2}} \right), \tag{3.2}$$

where $*$ is 2-D (x, t) convolution, travel time $\tau(x; z) = \dfrac{2}{v}\sqrt{x^2 + z^2}$ and $H(t)$ is the Heaviside function

$$H(t) = \begin{cases} 1, & t \geq 0, \\ 0, & t < 0. \end{cases}$$

Then

$$\begin{aligned} R(x, z) &= U(x, z; t = 0) = \frac{1}{\pi} \frac{\partial}{\partial z} \int dx_m \int_\tau^\infty \frac{U(x_m, 0; t')}{\sqrt{t'^2 - \tau^2}} dt' \\ &= \frac{1}{2\pi^2} \frac{\partial}{\partial z} \int dx_m \int_\tau^\infty \frac{dt'}{\sqrt{t'^2 - \tau^2}} \int e^{i\omega t'} \tilde{U}(x_m, 0; \omega) d\omega \\ &= \frac{1}{2\pi^2} \frac{\partial}{\partial z} \int dx_m \int \tilde{U}(x_m, 0; \omega) I(x_m, z; \omega) d\omega. \end{aligned} \tag{3.3}$$

where

$$I(x_m, z; \omega) = \int_\tau^\infty \frac{e^{i\omega t'}}{\sqrt{t'^2 - \tau^2}} dt' = \int_0^\infty \frac{e^{i\omega\sqrt{t^2 + \tau^2}}}{\sqrt{t^2 + \tau^2}} dt,$$

$\tau = \tau(x - x_m; z)$, and we have indicated the temporal Fourier transform of U by $\hat{U}$. Letting $\phi(t) = \sqrt{t^2 + \tau^2}$, we apply the method of stationary phase (Bleistein, 1984) to I, obtaining in the high-frequency limit

$$I(x_m, z; \omega) \sim \frac{1}{2\tau} e^{i\omega\tau} \sqrt{\frac{2\pi}{|\omega \phi''(0)|}} e^{i\frac{\pi}{4}\mathrm{sgn}(\omega)\mathrm{sgn}(\phi''(0))} = \frac{e^{i\omega\tau}}{2\sqrt{\tau}} \sqrt{-\frac{2\pi}{i\omega}}. \tag{3.4}$$

Since the stationary point $t = 0$ is an endpoint of integration, the denominator of this expression contains an extra factor of two. Substituting (3.4) into (3.3), we obtain

$$\begin{aligned} R(x, z) &\sim \frac{1}{(2\pi)^{3/2}} \frac{\partial}{\partial z} \int dx_m \int \tilde{U}(x_m, 0; \omega) \frac{e^{i\omega\tau}}{\sqrt{-i\omega\tau}} d\omega \\ &\sim \frac{1}{(2\pi)^{3/2}} \int dx_m \int \frac{z}{r} \sqrt{\frac{-2\omega i}{vr}} \tilde{U}(x_m, 0; \omega) e^{i\omega\tau} d\omega, \end{aligned} \tag{3.5}$$

where $r = \sqrt{(x - x_m)^2 + z^2}$.

Bleistein et al. (2000) have expressed 2-D true-amplitude zero-offset Kirchhoff migration as

$$R(x,z) \sim C \int dx_m \int \frac{z}{vr} |\omega| \tilde{P}(x_m;\omega) e^{i\omega\tau} d\omega, \tag{3.6}$$

where C is a constant and $P(x_m;t)$ is seismic data. Comparing (3.5) with (3.6), we see an amplitude and phase difference between zero-offset phase-shift migration and 2-D true-amplitude zero-offset Kirchhoff migration. In order to reconcile the two, we must apply some additional correction terms to the seismic data P, for example by setting

$$\tilde{U}(x_m,0;\omega) = \sqrt{i\omega}\sqrt{\frac{2r}{v}}\tilde{P}(x_m;\omega) \tag{3.7}$$

in (3.5). The first term in (3.7) is a phase correction to the input data, and the second term can be regarded as an amplitude compensation for geometrical spreading, which is conventionally applied in seismic data processing. We ignore constant multiplicative differences, which give rise only to different normalizations for the migrated output.

An equivalent way to implement the correction terms in (3.7) is to apply them in the pre-processing stage before phase-shift migration:

$$\tilde{U}(x_m,0;\omega) = \sqrt{i\omega}\int_0^\infty \sqrt{t} P(x_m;t) e^{-i\omega t} dt, \tag{3.8}$$

where t is two-way travel time which can be found in the seismic data. In short, pre-processing (3.8) together with Gazdag's phase shift migration (3.3) give Bleistein's true-amplitude zero-offset Kirchhoff migration.

A similar comparison of (3.5) with Bleistein et al.'s 2.5-D true-amplitude migration formula shows that we need to apply an amplitude compensation, but no phase compensation, to P before phase-shift migration in order to yield true 2.5-D amplitudes after 2-D migration.

4. Amplitudes in Dubrulle's migration formulas.

4.1. Amplitudes in Dubrulle's 2-D common-offset phase-shift migration. Just as Gazdag's zero-offset migration method has an implicit weight that can be compared with the true-amplitude Kirchhoff migration weight, so does Dubrulle's common-offset migration method. In this section, we derive expressions for these implicit weights in two dimensions, and compare them with Kirchhoff migration weights.

We begin by rewriting (2.1) with a $v(z)$ velocity function, setting $t = 0$ and using the inverse spatial Fourier transform of $\tilde{U}(x,0;\omega)$, as

$$R(x,z) = \frac{1}{(2\pi)^2}\int_{-\infty}^{+\infty} dx' \int_{-\infty}^{+\infty} d\omega \int_{-\frac{2|\omega|}{v}}^{\frac{2|\omega|}{v}} \tilde{U}(x',0;\omega) e^{i\omega t_0} e^{i(x-x')k_x} dk_x, \tag{4.1}$$

where

$$t_0 = \tau(x,x_m,z) - p_x(x_m - x) \qquad \text{and} \qquad p_x = -\frac{k_x}{\omega} = \frac{d\tau}{dx_m}.$$

Here, x_m and x are coordinates for the input and output, respectively. Applying the change of variable $k_x = \dfrac{2|\omega|}{v(z)}\sin\gamma(z)$, for $|\gamma| < \dfrac{\pi}{2}$, we obtain

$$R(x,z) = \frac{1}{(2\pi)^2}\iint d\omega dx' \int_{-\frac{\pi}{2}}^{\frac{\pi}{2}} \frac{2|\omega|}{v(z)} \tilde{U}(x',0;\omega) e^{i\omega\Phi(\gamma)} \cos\gamma d\gamma, \tag{4.2}$$

where

$$\Phi(\gamma) = \tau - p_x(x_m - x) + \frac{k_x}{\omega}(x - x') = \tau + \frac{2\mathrm{sgn}(\omega)\sin\gamma}{v(z)}(x_m - x'). \tag{4.3}$$

We plan to apply stationary phase to the γ-integral in (4.2); to that end, we show expressions for the first and second derivatives of Φ with respect to γ. The first derivative is

$$\frac{d\Phi}{d\gamma} = \frac{d\tau}{d\gamma} - (x_m - x')\frac{dp_x}{d\gamma} - p_x\frac{dx_m}{d\gamma} = -(x_m - x')\frac{dp_x}{d\gamma} = \frac{2\mathrm{sgn}(\omega)\cos\gamma}{v(z)}(x_m - x'), \tag{4.4}$$

so $x_m = x'$ is the stationary point. A much more detailed analysis, presented in Appendix A, shows that

$$\left.\frac{d^2\Phi}{d\gamma^2}\right|_{x_m = x'} = -4\frac{\cos^2\gamma(z)}{v^2(z)}\left(\frac{\cos\alpha_s(z)}{\psi_s} + \frac{\cos\alpha_r(z)}{\psi_r}\right)^{-1}, \tag{4.5}$$

where

$$\psi_s = \cos\alpha_s(z)\int_0^z \frac{v(z')}{\cos^3\alpha_s(z')}dz' \quad \text{and} \quad \psi_r = \cos\alpha_r(z)\int_0^z \frac{v(z')}{\cos^3\alpha_r(z')}dz'$$

are in-plane geometrical spreading terms from sources and receivers, respectively. The number α_s (α_r) is the angle along the ray path from source (receiver) relative to the vertical (Figure 2).

Now applying stationary phase to (4.2), we obtain the following integral form for Dubrulle's phase-shift migration

$$R(x,z) \sim \frac{1}{(2\pi)^{\frac{3}{2}}}\iint \sqrt{-i\omega}\sqrt{\frac{\cos\alpha_r}{\psi_r} + \frac{\cos\alpha_s}{\psi_s}}\tilde{U}(x_m, 0; \omega)e^{i\omega\tau(z)}d\omega dx_m. \tag{4.6}$$

Remark 4.1. For zero-offset and constant velocity, we have the explicit expressions

$$\frac{\cos\alpha_s}{\psi_s} = \frac{\cos\alpha_r}{\psi_r} = \frac{z^2}{vr^3}.$$

Substituting these into (4.6), we obtain the integral form of phase-shift migration (3.5) derived earlier.

4.2. Comparison with true-amplitude Kirchhoff migration. 2-D true-amplitude common-offset migration for a $v(z)$ medium can be expressed as (Martins et al., 1997; Hanitzsch, 1997; Zhang et al., 2000)

$$R(x,z) \sim C\iint |\omega|\frac{\sqrt{\cos\alpha_{s0}\cos\alpha_{r0}}}{v(0)}\left(\sqrt{\frac{\psi_s}{\psi_r}} + \sqrt{\frac{\psi_r}{\psi_s}}\right)\tilde{P}(x_m;\omega)e^{i\omega\tau(z)}d\omega dx_m. \tag{4.7}$$

As in the discussion in Section 3, in order to make the amplitude and phase of the migration in (4.6) identical, up to a multiplicative constant, with those of (4.7), we need to apply some pre-processing to the seismic data P. In this case, we set

$$\tilde{U}(x_m, 0; \omega) = \sqrt{i\omega}\int_0^\infty LP(x_m; t)e^{-i\omega t}dt, \tag{4.8}$$

before applying phase-shift migration, where L is a geometrical spreading correction term to be determined.

Now we ask, can we make Dubrulle's migration true-amplitude if we play the same game as we did to zero-offset phase-shift migration? To answer this question, we will discuss three typical cases.

Cases 1 and 2: $v(z)$, flat events or zero offset. In both cases $\alpha_s = \alpha_r = \alpha$ and $\psi_s = \psi_r = \psi$, therefore the true-amplitude weight for Kirchhoff migration (4.7) is

$$W_{\mathrm{TA}} = \frac{2\cos\alpha_0}{v(0)}.$$

Ursin (1990) derived an expression for 3-D geometrical spreading correction in a layered medium (his Eq. (8)). By dropping the out-of-plane term in Ursin's expression, we obtain the following 2-D correction term:

$$L = \frac{\cos\alpha_0}{v(0)}\sqrt{\frac{2\psi}{\cos\alpha}}.$$

As Ursin (1990) showed (his Eq. (12)), this factor can be written as a function of offset h and two-way travel time t, making it appropriate to apply to $P(x;t)$ before transformation to $\hat{U}$ and subsequent phase-shift migration to a particular depth. Multiplying the factor L by the weight in (4.6), we obtain the following total weight for Dubrulle's migration:

$$W_{\mathrm{D}} = L\sqrt{\frac{2\cos\alpha}{\psi}} = \frac{2\cos\alpha_0}{v(0)} = W_{\mathrm{TA}},$$

showing that this correction, applied to input data P, will provide correctly weighted input data for either zero-offset phase-shift migration at arbitrary dip or nonzero-offset phase-shift migration at flat dips.

Case 3: Constant velocity and common offset. For constant velocity,

$$\cos\alpha_s = \frac{z}{r_s}, \qquad \cos\alpha_r = \frac{z}{r_r}$$

and

$$\psi_s = \frac{vr_s^2}{z}, \qquad \psi_r = \frac{vr_r^2}{z}.$$

The true-amplitude migration weight is then

$$W_{\mathrm{TA}} = \frac{z}{v}\frac{r_s^2 + r_r^2}{(r_s r_r)^{3/2}}, \tag{4.9}$$

where r_s and r_r are distances from the diffractor to the source and receiver, respectively.

In cases 1 and 2, multiplying the implicit phase-shift migration weight by the geometrical spreading correction L yielded the true-amplitude Kirchhoff migration weight. The present case is not so simple. Here, the quotient of W_{TA} and W_{D} includes r_s and r_r, which depend on the source and receiver ray paths. It can not be expressed as a simple correction applicable to the input data in either the time domain or the space domain, nor is it exactly equal to the geometrical spreading correction L. Still, we can multiply the input data by L before Fourier transforming it into the frequency domain in order to approximate the desired quotient, and this approximation is surprisingly accurate as we will show below. The geometrical correction term is

$$L = \sqrt{\frac{r_s + r_r}{v}} = \sqrt{t}. \tag{4.10}$$

We obtain the effect of this on the total weight $W_{\rm D}$ by substituting (4.10) into (4.8) and combining with (4.6):

$$W_{\rm D} = L\frac{z}{\sqrt{v}}\sqrt{\frac{1}{r_s^3}+\frac{1}{r_r^3}} = \frac{z}{v}\frac{\sqrt{(r_s^3+r_r^3)(r_s+r_r)}}{(r_s r_r)^{3/2}}. \tag{4.11}$$

Comparing (4.9) with (4.11), we find that

$$W_{\rm D} = W_{\rm TA}\frac{\sqrt{(r_s^3+r_r^3)(r_s+r_r)}}{r_s^2+r_r^2} \geq W_{\rm TA}, \tag{4.12}$$

so that the equivalent Kirchhoff weight for Dubrulle's migration is always larger than the true-amplitude migration weight, with equality if and only if $r_s = r_r$, i.e. in the case of zero-offset or flat reflector. So generally, Dubrulle's migration is not true-amplitude. Figure 3 illustrates the relative error

$$E = \frac{|W_{\rm TA} - W_{\rm D}|}{W_{\rm T}}.$$

From Figure 3, we see that the amplitude error in Dubrulle's method with the time scaler (4.10) applied to $P(x_m;t)$ is relatively small, less than 6.1%. Indeed, the maximum relative error

$$E_{\max} = 0.060660171\ldots,$$

occurs when

$$r_s = (2+\sqrt{3})r_r \qquad \text{or} \qquad r_r = (2+\sqrt{3})r_s.$$

5. Amplitude behavior in (generalized) Dubrulle's 3-D migration . In Section 2, we generalized Dubrulle's migration to 3-D common-offset, common-azimuth data volumes. As in 2-D, a similar but more complicated analysis can be applied to algorithm (2.2). Here we just give the final result, without showing details of the derivation:

$$R(x,y,z) \sim -\frac{1}{(2\pi)^2}\iiint W_{\rm D} i\omega\tilde{P}(x_m,y_m;\omega)e^{i\omega\tau}d\omega dx_m dy_m, \tag{5.1}$$

where the amplitude weight

$$W_{\rm D} = L\sqrt{\left(\frac{1}{\sigma_s}+\frac{1}{\sigma_r}\right)\left(\frac{\cos\alpha_s}{\psi_s}+\frac{\cos\alpha_r}{\psi_r}\right)+\sin^2\lambda\left(\frac{1}{\sigma_s}-\frac{\cos\alpha_s}{\psi_s}\right)\left(\frac{1}{\sigma_r}-\frac{\cos\alpha_r}{\psi_r}\right)}. \tag{5.2}$$

Here, L is the geometrical correction term, λ is the angle between the projection of source and receiver rays to the surface (Figure 4) , and

$$\sigma_s = \int_0^z \frac{v(z')}{\cos\alpha_s(z')}dz' \qquad \text{and} \qquad \sigma_r = \int_0^z \frac{v(z')}{\cos\alpha_r(z')}dz'$$

are out-of-plane spreading terms. In 3-D, the phase correction term is no longer needed.

For a $v(z)$ medium, the true-amplitude Kirchhoff migration weight (Winbow and Schneider, 1999; Zhang et al., 2000) is

$$W_{\rm TA} = \frac{\sqrt{\cos\alpha_{s0}\cos\alpha_{r0}}}{v_0}\left[\left(\sqrt{\frac{\psi_s}{\psi_r}}+\sqrt{\frac{\psi_r}{\psi_s}}\right)\left(\sqrt{\frac{\sigma_s}{\sigma_r}}+\sqrt{\frac{\sigma_r}{\sigma_s}}\right)+\frac{\sin^2\lambda}{2\cos^2\theta}Q\right], \tag{5.3}$$

where

$$Q = (\cos\alpha_s + \cos\alpha_r)\left(\sqrt{\frac{\psi_s\psi_r}{\sigma_s\sigma_r}} + \sqrt{\frac{\sigma_s\sigma_r}{\psi_s\psi_r}}\right) - (1 + \cos\alpha_s\cos\alpha_r)\left(\sqrt{\frac{\psi_s\sigma_r}{\psi_r\sigma_s}} + \sqrt{\frac{\psi_r\sigma_s}{\psi_s\sigma_r}}\right),$$

and θ is the reflection angle.

Cases 1 and 2: $v(z)$, flat events or zero offset. For zero offset, the opening angle 2θ is zero and therefore its projection λ is also zero. For a flat reflector, the specular ray pair is restricted to the vertical plane below the source and receiver locations, therefore the projection of the opening angle is 180°. In both cases $\sin\lambda = 0$, so

$$W_{\mathrm{TA}} = \frac{4\cos\alpha_0}{v(0)}.$$

Applying Ursin's (1990) 3-D geometrical spreading correction

$$L = \frac{2\cos\alpha_0}{v(0)}\sqrt{\frac{\sigma\psi}{\cos\alpha}}$$

to W_{D} in (5.2), we obtain

$$W_{\mathrm{D}} = 2\sqrt{\frac{\cos\alpha}{\sigma\psi}}L = \frac{4\cos\alpha_0}{v(0)} = W_{\mathrm{TA}},$$

so that 3-D $v(z)$ common-offset, common-azimuth migration can provide true amplitudes at zero-offset or for flat reflectors.

Case 3: constant velocity, common offset, and common azimuth. As in 2-D, this case is more complicated than the preceding cases. Here,

$$W_{\mathrm{D}} = L\frac{z}{v}\frac{\sqrt{(r_s + r_r)(r_s^3 + r_r^3)}}{(r_s r_r)^2},$$

and

$$W_{\mathrm{TA}} = \frac{z}{v}\frac{(r_s^2 + r_r^2)(r_s + r_r)}{(r_s r_r)^2}.$$

As in 2-D, the quotient of W_{TA} and W_{D} can not be expressed as a function that can multiply the input data in either the time domain or the space domain, nor does it equal L. But applying the geometrical spreading correction

$$L = r_s + r_r = vt$$

to the input data in the time domain yields the approximate total weight for Dubrulle's migration

$$W_{\mathrm{D}} = \frac{z}{v}\frac{\sqrt{(r_s + r_r)^3(r_s^3 + r_r^3)}}{(r_s r_r)^2}.$$

Therefore, as in 2-D, we obtain the relationship

$$W_{\mathrm{D}} = W_{\mathrm{TA}}\frac{\sqrt{(r_s^3 + r_r^3)(r_s + r_r)}}{r_s^2 + r_r^2} \geq W_{\mathrm{TA}}, \tag{5.4}$$

which is exactly the same as its 2-D case (4.12).

6. Amplitudes and anti-aliasing. In previous sections, we discussed the amplitude performance of Dubrulle's phase-shift migration. In migration practice, anti-aliasing modifies migrated amplitudes also, by reducing the frequency content of an input trace as it migrates to steeper angles.

Two kinds of aliasing happen to Kirchhoff migration (Lumley et al., 1994) : operator aliasing and imaging aliasing. Operator aliasing occurs when the dip along the migration summation trajectory is too steep for a given input trace spacing and frequency content. As a result, not all the unwanted smile energy cancels, and we may be left with the envelope plus some unwanted noise. Imaging aliasing occurs when the output sampling is too coarse to properly present migrated dips. Such aliasing changes the appearance of dipping events on a migrated section and may mislead interpretation of imaging.

In phase-shift migration, input trace spacings, dx and dy, are always the same as output spacings, so the following formula for the highest frequency controls both operator aliasing and imaging aliasing (Zhang et al., 2001)

$$f_{\max} = \frac{1}{2 \max \left\{ \left| \frac{\partial \tau}{\partial x} \right| dx, \left| \frac{\partial \tau}{\partial y} \right| dy \right\}}, \tag{6.1}$$

Equation (6.1) can be used to predict the amplitude decay caused by anti-aliasing in phase-shift migration (Figure 5). Figure 6 shows the effects of anti-aliasing on migrated impulses. In the examples, we assume that the input wavelet is a sinc function with a maximum frequency of 50hz, we choose $v = 2000$m/s, $dx = 25$m, and we vary the offset from 0m to 6000m. Because the input data have frequency content above the aliasing frequency $v/(4dx) = 20$hz, migration (even with anti-aliasing) will fail to resolve the true dip of steeply dipping events, migrating their actual and aliased dip components without completely cancelling the aliased components. Also, while anti-aliasing has no effect on the amplitudes of events whose frequency content is below the aliasing frequency, the migrated amplitudes of events with frequency content above the aliasing frequency will be affected by anti-aliasing at steep enough dips. For this example, Figure 6 shows that amplitude loss at a dip angle, proportional to the decrease in maximum frequency migrated to that dip, ranges between 0% and 60%, and that this loss is not the same for all offsets. Over most of the migrated smile, the amplitude decay from anti-aliasing is much larger than the amplitude error (0%-6.1%) from Dubrulle's phase-shift migration.

We analyze anti-aliasing as a function of offset and reflector azimuth from the following equations, valid for a $v(z)$ medium,

$$\frac{\partial \tau}{\partial x} = \frac{2 \cos\theta \sin\delta}{v} \cos\mu \qquad \text{and} \qquad \frac{\partial \tau}{\partial y} = \frac{2 \cos\theta \sin\delta}{v} \sin\mu, \tag{6.2}$$

where θ is incidence angle, δ is dip angle and μ is reflector azimuth angle. Substituting these into (6.1), we obtain

$$f_{\max} = \frac{v}{4 \cos\theta \sin\delta \max\{|\cos\mu| dx, |\sin\mu| dy\}}. \tag{6.3}$$

This expression shows that, for a given dip rate and fixed azimuth, anti-aliasing affects different offsets differently, typically attenuating amplitudes at near offsets (i.e., small incidence angles) more than it attenuates far-offset amplitudes (see Figure 7). Alternatively, fixing δ and varying μ gives the dependence of anti-aliasing on azimuth, and can be used to determine amplitude loss due to anti-aliasing as a function of azimuth. From Eq. (6.3) we see that anti-aliasing affects the analysis of amplitudes on migrated gathers, often more than the choice of migration weights does.

7. Conclusions. The speed of common-offset, common-azimuth $v(z)$ phase-shift migration makes it an attractive alternative to Kirchhoff migration in areas of moderate structural complexity. Its amplitude fidelity, however, is theoretically less than that of true-amplitude Kirchhoff migration unless its implicit weights are replaced with Kirchhoff migration weights. To do this for a general $v(z)$ medium, it is necessary to recast phase-shift migration as the Fourier transform of a true-amplitude Kirchhoff migration algorithm, performing appropriate asympotics along the way (Etgen, 1998). Even when this is done, the anti-aliasing which is implicit in phase-shift migration will reduce the migrated amplitudes from their correct values. These amplitude errors are more severe for near offsets than far offsets, making post-migrated AVO problematic, particularly for shallow reflection events.

Appendix A. Derivation of equation (4.5).

Differentiating Eq. (4.4) with respect to γ, we obtain

$$\left.\frac{d^2\Phi}{d\gamma^2}\right|_{x_m=x} = 2\mathrm{sgn}(\omega)\frac{\cos\gamma(z)}{v(z)}\frac{dx_m}{d\gamma}. \tag{A.1}$$

In the following, we attempt to find an explicit expression for $\dfrac{dx_m}{d\gamma}$.

In a $v(z)$ medium, we have the following relationships

$$x - x_m = \frac{1}{2}\left(\int_0^z \tan\alpha_r(z')dz' - \int_0^z \tan\alpha_s(z')dz'\right), \tag{A.2}$$

$$h = \frac{1}{2}\left(\int_0^z \tan\alpha_r(z')dz' + \int_0^z \tan\alpha_s(z')dz'\right), \tag{A.3}$$

and

$$\tau(x, x_m; z) = \int_0^z \frac{ds}{v(z')\cos\alpha_s(z')} + \int_0^z \frac{ds}{v(z')\cos\alpha_r(z')}. \tag{A.4}$$

Differentiating (A.4) with respect to x_m, and applying (A.2) and (A.3), we obtain

$$2\mathrm{sgn}(\omega)\frac{\sin\gamma(z)}{v(z)} = -p_x = -\frac{d\tau}{dx_m} = \frac{\sin\alpha_r(z)}{v(z)} - \frac{\sin\alpha_s(z)}{v(z)}. \tag{A.5}$$

By using Snell's law, we know that

$$\frac{\sin\alpha_s(z')}{v(z')} = \frac{\sin\alpha_s(z)}{v(z)} \quad \Rightarrow \quad d\alpha_s(z') = \frac{v(z')\cos\alpha_s(z)}{v(z)\cos\alpha_s(z')}d\alpha_s(z), \tag{A.6}$$

$$\frac{\sin\alpha_r(z')}{v(z')} = \frac{\sin\alpha_r(z)}{v(z)} \quad \Rightarrow \quad d\alpha_r(z') = \frac{v(z')\cos\alpha_r(z)}{v(z)\cos\alpha_r(z')}d\alpha_r(z). \tag{A.7}$$

Differentiating (A.2) and (A.3) with respect to γ, and combining with (A.6) and (A.7), we have

$$\begin{aligned}
\frac{dx_m}{d\gamma} &= -\frac{d(x - x_m)}{d\gamma} = -\frac{1}{2}\frac{d}{d\gamma}\left(\int_0^z \tan\alpha_r(z')dz' - \int_0^z \tan\alpha_s(z')dz'\right) \\
&= \frac{1}{2}\left(\int_0^z \frac{1}{\cos^2\alpha_s(s)}\frac{d\alpha_s(z')}{d\gamma}dz' - \int_0^z \frac{1}{\cos^2\alpha_r(z')}\frac{d\alpha_r(z')}{d\gamma}dz'\right) \\
&= \frac{\psi_s}{2v(z)}\frac{d\alpha_s(z)}{d\gamma} - \frac{\psi_r}{2v(z)}\frac{d\alpha_r(z)}{d\gamma},
\end{aligned} \tag{A.8}$$

and

$$\begin{aligned} 0 = \quad & \frac{dh}{d\gamma} = \frac{1}{2}\left(\int_0^z \frac{1}{\cos^2\alpha_r(z')}\frac{d\alpha_r(z')}{d\gamma}dz' + \int_0^z \frac{1}{\cos^2\alpha_s(z')}\frac{d\alpha_s(z')}{d\gamma}dz'\right) \\ = \quad & \frac{\psi_s}{2v(z)}\frac{d\alpha_r(z)}{d\gamma} + \frac{\psi_r}{2v(z)}\frac{d\alpha_s(z)}{d\gamma}. \end{aligned} \tag{A.9}$$

Differentiating both sides of (A.5) with respect to γ, we obtain another useful relation:

$$2\mathrm{sgn}(\omega)\cos\gamma = \cos\alpha_r(z)\frac{d\alpha_r(z)}{d\gamma} - \cos\alpha_s(z)\frac{d\alpha_s(z)}{d\gamma}. \tag{A.10}$$

From (A.9) and (A.10), we can solve for $\frac{d\alpha_r(z)}{d\gamma}$ and $\frac{d\alpha_s(z)}{d\gamma}$, and then substitute them into (A.8) to obtain

$$\frac{dx_m}{d\gamma} = -\frac{2\mathrm{sgn}(\omega)\cos\gamma}{v(z)}\left(\frac{\cos\alpha_s(z)}{\psi_s} + \frac{\cos\alpha_r(z)}{\psi_r}\right)^{-1}, \tag{A.11}$$

which gives (4.4) together with (A.1).

References

Bleistein, N., Cohen, J. K., and Stockwell, J. W., 2000, Mathematics of multidimensional seismic inversion: Springer.

Bleistein, N., 1984, Methematical methods for wave phenomena: Academic Press, Inc.

Dubrulle, A. A., 1983, Numerical methods for the migration of constant-offset sections in homogeneous and horizontally layered media: Geophysics, **48**, 1195–1203.

Ekren, B. O., and Ursin, B., 1999, True-amplitude frequency-wavenumber constant-offset migration: Geophysics, **64**, 915–924.

Etgen, J. T., 1998, $v(z)$ prestack migration of common-offset common-azimuth data volumes, part 1: Theory: 68th Ann. Mtg., Soc. Expl. Geophys., Expanded Abstracts, pages 1835–1838.

Gazdag, J., 1978, Wave equation migration with the phase-shift method: Geophysics, **43**, 1342–1351.

Gray, S. H., 1992, Frequency-selective design of the Kirchhoff migration operator: : Geophys. Prosp., **40**, 565–572.

Hanitzsch, C., 1997, Comparison of weights in prestack amplitude-preserving Kirchhoff depth migration: Geophysics, **62**, no. 6, 1812–1816.

Lumley, D. E., Claerbout, J. F., and Bevc, D., 1994, Anti-aliased Kirchhoff 3-D migration: 64th Ann. Mtg., Soc. Expl. Geophys., Expanded Abstracts, pages 1282–1285.

Martins, J., Schleicher, J., Tygel, M., and Santos, L., 1997, 2.5-D true-amplitude migration and demigration: Joutnal of Seismic Exploration, **6**, no. 2/3, 159–180.

Schleicher, J., Tygel, M., and Hubral, P., 1993, 3-D true amplitude finite-offset migration: Geophysics, **58**, no. 8, 1112–1126.

Ursin, B., 1990, Offset-dependent geometrical spreading in a layered medium: Geophysics, **55**, no. 4, 492–496.

Winbow, G., and Schneider, W., 1999, Weights for 3-D controlled amplitude prestack time migration: 69th Annual Internat. Mtg., Soc. Expl. Geophys., Expanded Abstracts, pages 1110–1113.

Zhang, Y., Gray, S., and Young, J., 2000, Exact and approximate weights for Kirchhoff migration: 70th Ann. Mtg., Soc. Expl. Geophys., Expanded Abstracts, pages 1036–1039.

Zhang, Y., Gray, S., Sun, J., and Notfors, C., 2001, Theory of migration anti-aliasing: 71th Ann. Mtg., Soc. Expl. Geophys., Expanded Abstracts, pages 997–1000.

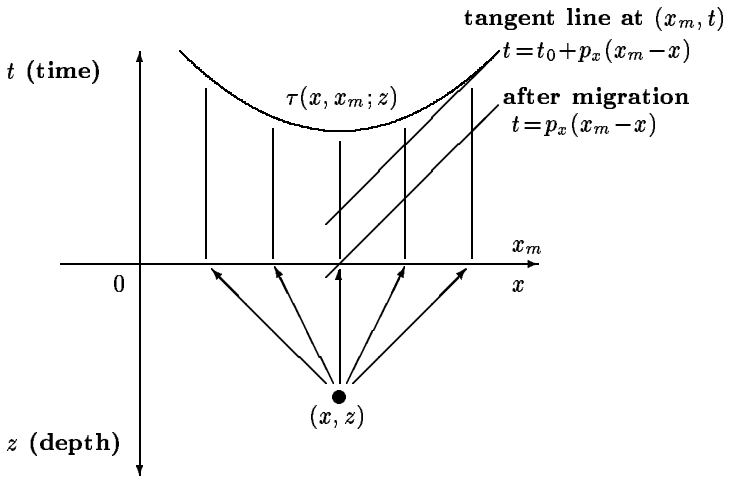

FIG. 1. *Dubrulle's principle of prestack migration. The plane-wave component of the data tangent to the diffraction curve at* (x_m, t) *is accumulated into the image at* (x, z).

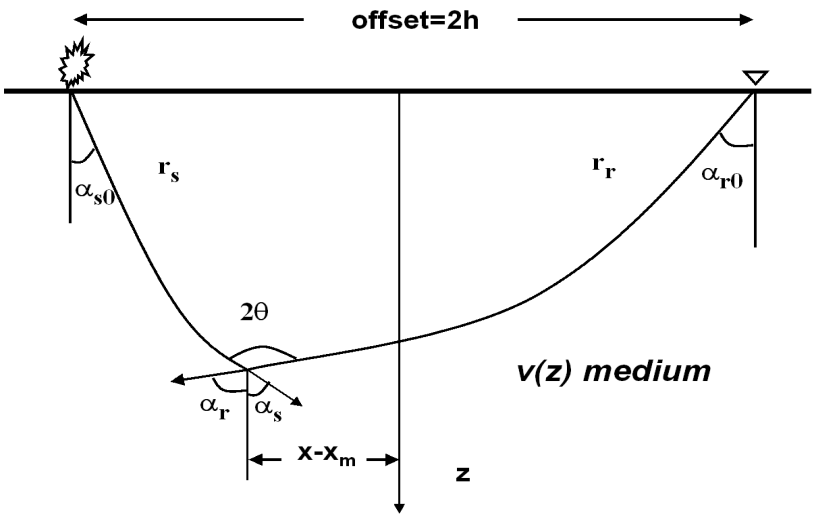

FIG. 2. *Ray paths in a $v(z)$ medium.*

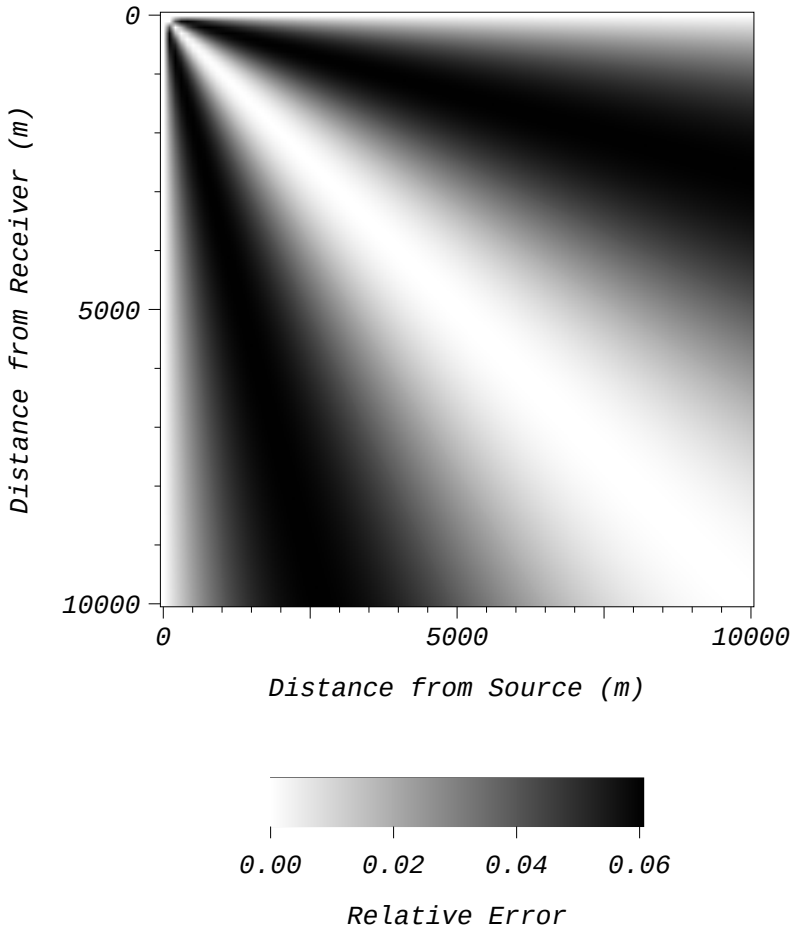

FIG. 3. *Relative amplitude error of Dubrulle's migration.*

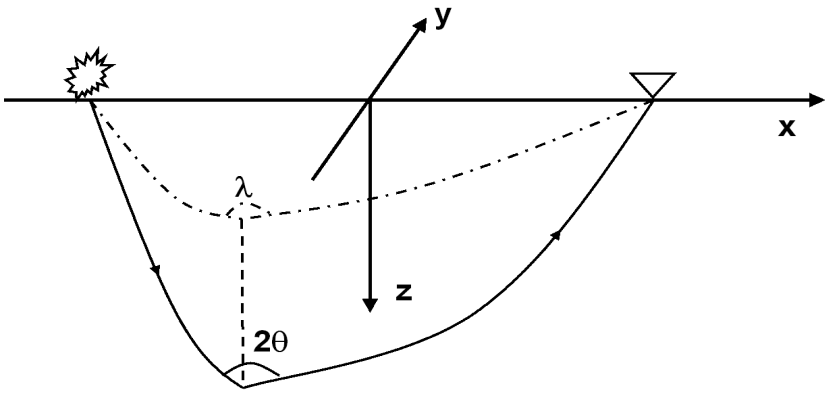

FIG. 4. *Definitions of λ and θ in 3-D amplitude weights. 2θ is the opening angle, i.e. the angle between the ray from the source and the ray from the receiver, and λ is its projection on the plane $z = 0$.*

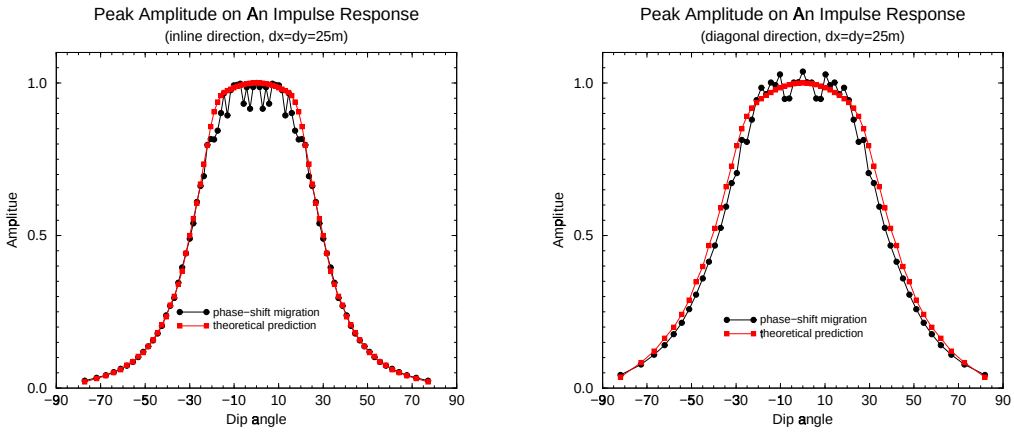

FIG. 5. *Peak amplitudes on an impulse (30hz Ricker Wavelet) response of zero-offset phase-shift migration ($dx = dy = 25m$) vs. predicted amplitudes using Eq.* (6.1). *Left: central subline; Right: central diagonal line.*

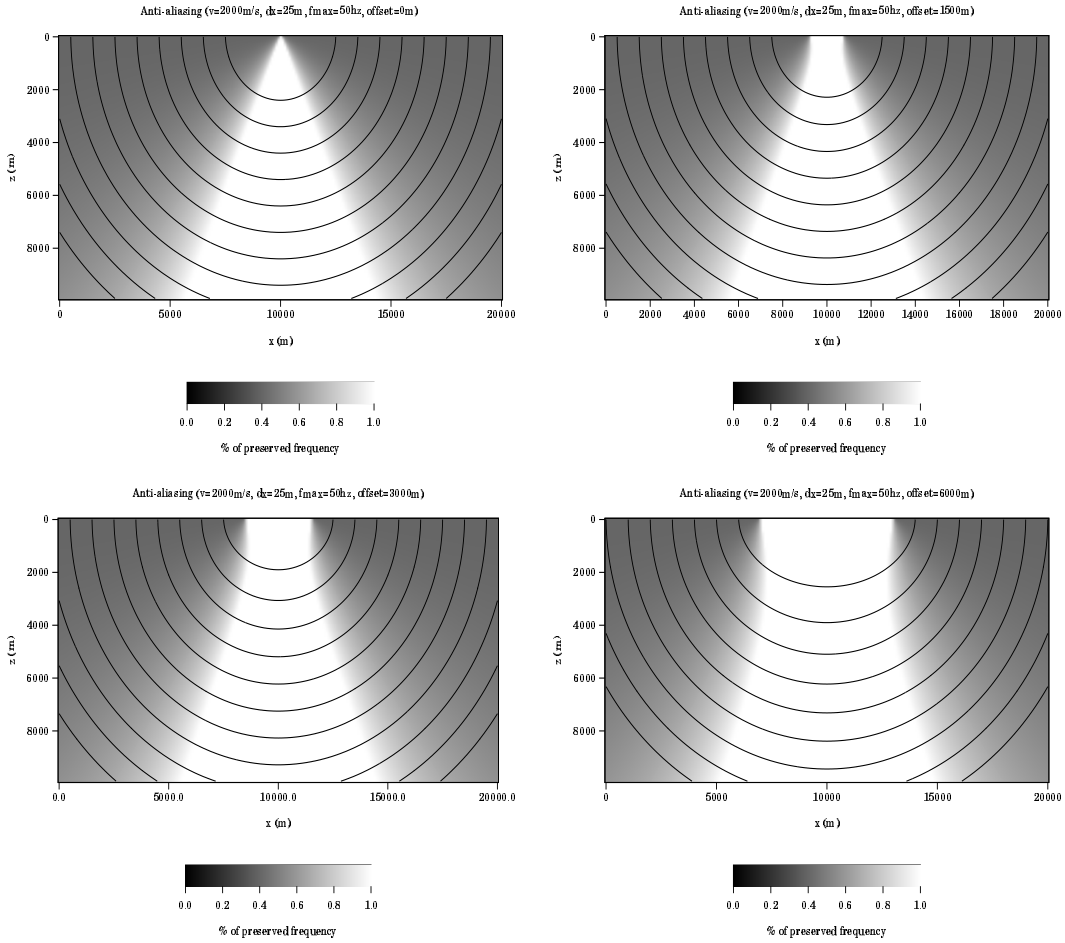

FIG. 6. *Anti-aliasing vs. offset, using Eq.* (6.1).

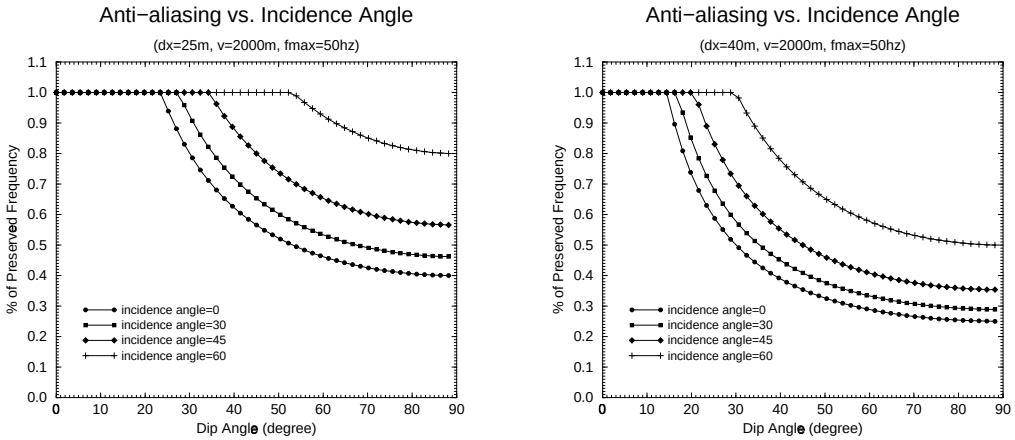

FIG. 7. *Anti-aliasing vs. incidence angle. The input is supposed to have highest frequency* $f_{\max} = 50hz$, $v = 2km/s$, $dx = 25m$ *(left) and* $40m$ *(right). The frequency losses are calculated using Eq.* (6.3). *Four incidence angles* (0°, 30°, 45° *and* 60°) *are shown. Note: for constant velocity, incidence angle always increases with offset.*